










## Article

# Improvement and impacts of forest canopy parameters on Noah-MP land surface model from UAV-based photogrammetry

Ming Chang<sup>1</sup>, Shengjie Zhu<sup>2</sup>, Jiachen Cao<sup>1</sup>, Bingyin Chen<sup>1</sup>, Qi Zhang<sup>3</sup>, Weihua Chen<sup>1</sup>, Shiguo Jia<sup>3</sup>, Padmaja Krishnan<sup>4</sup> and Xuemei Wang<sup>1,\*</sup>

<sup>1</sup> Guangdong-Hongkong-Macau Joint Laboratory of Collaborative Innovation for Environmental Quality, Institute for Environmental and Climate Research, Jinan University, Guangzhou, China

<sup>2</sup> Department of Environmental Science, Guangdong Polytechnic of Environmental Protection Engineering, Foshan, China

<sup>3</sup> Guangdong Province Key Laboratory for Climate Change and Natural Disaster Studies, School of Atmospheric Sciences, Sun Yat-sen University, Guangzhou, China

<sup>4</sup> Department of Civil & Environmental Engineering, National University of Singapore, Singapore, Singapore

\* Correspondence: [eciwxm@jnu.edu.cn](mailto:eciwxm@jnu.edu.cn)

**Abstract:** Taking a typical forest underlying surface as the research area, this study employed the unmanned aerial vehicle (UAV) photogrammetry to explore more accurate canopy parameters including tree height and canopy radius, which were used to improve the Noah-MP land surface model conducted in Dinghushan Forest Ecosystem Research Station (CN-Din). While the canopy radius was fitted as a Burr distribution, the canopy height of CN-Din forest followed a Weibull distribution. The replacement of the parameters by these observed UAV would result in the Noah-MP model. It was found that the influence on the simulation of the energy fluxes could not be negligible, and the main influence of these canopy parameters was on the latent heat flux which could decrease up to -11% in the midday while increase up to 15% in the nighttime. Additionally, this work indicated that the description of the canopy characteristics for the land surface model should be improved to accurately deliver the heterogeneity for the underlying surface.

**Keywords:** forest canopy parameters; UAV-based photogrammetric; land surface modelling

## 1. Introduction

The land surface process is the lower boundary condition of atmospheric movement, and the different types of underlying surface have multiple weather and climate effects [1]. It has been known that the differences of underlying surface characteristics are embodied by using different land surface parameters [2]. Generally, the measurement of pollutant deposition and the estimation of ecological impact depend on the accuracy of the simulation results of land-air exchange flux, thus the improvement of canopy properties are urgently needed in modelling land-atmosphere interaction processes [3].

Additionally, the performance of the land surface models and the coupled atmosphere & environment models can be improved by the refined land surface inputs and parameters [4]. However, the treatment of vegetation, especially the forest canopy structure, has been set as a big-leaf in land surface models for a long time [5]. Although some 3-D computer simulation models have been suitable for studying the smaller scale scenes with fine structures, the demands of extreme computational resources still made it difficult to apply in a large scale [6]. In this case, the range of typical parameter values on forest remains a large source of uncertainty [3].

The parameterizations about forest canopy structure of land surface models which are commonly coupled in the meteorological or climate simulation are listed in Table 1 [7–13]. Different parameterization schemes divide the canopy into one layer, two layers or multi layers to calculate

the energy decomposition or radiative transfer in the canopy [14–17]. For the calculation of the atmospheric dynamic process, the current land surface models which have been widely used in climate and hydrology researches, such as simple biosphere model (SiB4) and biosphere atmosphere transfer scheme (BATS), are based on the measured empirical wind speed profile in the canopy to provide an empirical solution to calculate the turbulent exchange in the canopy [18,19].

**Table 1.** Forest Canopy Parameterization in Land Surface Models

Land Surface Models	Noah	Noah-MP	CLM	RUC	SSiB	PX
Vegetative components	one vegetation type in one gridcell without dynamic vegetation and carbon budget	one vegetation type in one gridcell with dynamic vegetation and carbon budget	subgrids with up to 10 vegetation types in one gridcell with dynamic vegetation and carbon budget	multiple vegetation type by using landuse fraction in one gridcell without dynamic vegetation and carbon budget	one vegetation type in one gridcell without dynamic vegetation and carbon budget	one vegetation type in one gridcell without dynamic vegetation and carbon budget
Photosynthetic pathway	No	Yes, ¶ = 1	Yes, ¶ = 1	No	No	Yes, § = 1
Phenology	Yes, ¶ = 1	Yes, § = 1	Yes, † = 1	Yes, ¶ = 1	No	Yes, ¶ = 1
Relative leaf nitrogen profile	No	Yes, ¶ = 2	Yes, § = 1	No	No	No
Leaf dimension	No	No	Yes, ¶ = 1	No	Yes, ¶ = 1	No
Leaf area index	Yes, ¶ = 1	Yes, ¶ = 2	Yes, ¶ = 2	Yes, ¶ = 2	Yes, ¶ = 1	Yes, § = 1
Canopy heights	Yes, ¶ = 2	Yes, ¶ = 2	Yes, ¶ = 2	No	Yes, ¶ = 1	No
Length of live crown	No	No	No	No	No	No
Length of dead crown	No	No	No	No	No	No
Crown radius	No	Yes, ¶ = 1	Yes, ¶ = 1	No	No	No
Number of branches	No	Yes, ¶ = 1	No	No	No	No
Branch zenith	No	No	No	No	No	No

¶: Number of Parameters

§: Using Subroutines

†: Using Modules (multiple subroutines)

Unmanned aerial vehicle (UAV) provides an effective platform for quickly and cheaply obtaining the parameters of vegetation canopy [20]. This technique has been expected to become increasingly common in forests studies with the availability of more efficient data processing software [21,22]. The communities start using UAVs to map canopy gaps, tree heights and leaf angle etc. [23–26], but the performance on simulating mass and energy exchanges between ecosystems and the atmosphere in land surface models still needs further exploration.

In this study, a typical subtropical forest underlying surface was taken as the research area, and we managed to establish a fast and cheap method to obtain accurate canopy parameters including tree heights and crown radius of this forest by UAV photogrammetry. Finally, with these parameters to replace the original default value of model, the difference of simulated heat flux caused by using these accurately obtained canopy parameters was explored.

## 2. Method

### 2.1. Study Area and Field Data Collection

The study was carried out in the Dinghushan Forest Ecosystem Research Station, which could represent the subtropical forest areas in South China (Fluxnet Site Code: CN-Din). This site is located in Dinghushan biosphere reserve of Zhaoqing, Guangdong province, China (as shown in Figure 1, also in Chang *et al.* [27]). The majority of the area is covered by a 100 year old subtropical evergreen broadleaf and pine-broadleaf mixed forest, mainly consisting of *Castanopsis chinensis*, *Schima superba* and *Pinus massoniana*, etc [28,29]. The vegetation is fairly homogeneous within the distance of ~1 km in the direction of the dominant wind direction (Northeast). The measurements of UAV photographs were performed from August 2019 to September 2019, representing a comprehensive observation experiment of dry deposition measurement in CN-Din [30].

### 2.2. Workflow from UAV Photography to Land-Atmospheric Simulation

A general workflow was established to calculate the tree height and the crown radius (as shown in Figure 2). Most of the procedures were carried out using the new automatic tools and algorithms [31]. A 3D reconstruction terrain-oriented software was employed to create the point clouds and orthomosaics from a set of images on the same subject, by means of structure from motion (SfM) techniques [32].

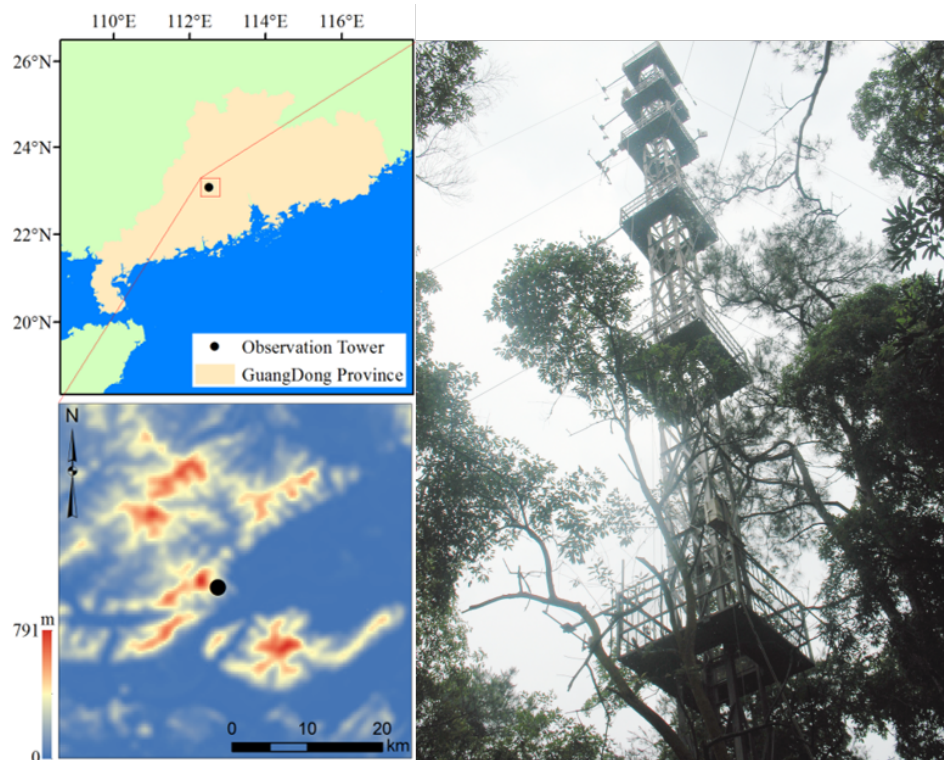


**Figure 1.** Location and geographic features of Dinghushan station

The average flight altitude for this study was set at 100 meters but varied because of relief (as shown in Figure 3). This resulted in photographs with a ground sample distance (GSD) of 7.2 cm on average. The flight lines were programmed for the images to have a 85% overlap in flight direction and 60% side overlap. This sparse point cloud was then used to create a dense point cloud with mean point density of 42.6 points/m for the 100 m high flights. Then, a canopy height model represented the difference between a digital terrain model and surface model. Finally, the parameters of the canopy that included tree height and tree radius were built from this point cloud.

### 2.3. Land Surface Model Setup

In this work, we chose Noah-MP land surface model to estimate the effects of the updated parameters. This model, a state-of-the-art, consists of 12 biophysical and hydrological processes that control heat fluxes between the surface and the atmosphere. Additionally, these processes also include dynamic vegetation, stomatal conductance, surface exchange coefficients for heat and water vapor, radiation interactions with the vegetation canopy and the soil, hydrological processes within the canopy and the soil, a multi-layer snowpack, frozen ground and aquifer model for groundwater dynamics [11].

On the other hand, due to the lack of observed surface heat flux data during the UAV flight, we evaluate the simulation impact of UAV-based parameters by using the validated benchmark observation dataset which has been analyzed in our previous study, i.e. Zhang *et al.* [33]. Table 2 shows the setup of option combinations which were verified and chosen by an ensemble simulation test [27]. The average monthly diurnal LH and SH obtained from observations and simulated from the option combinations in the previous paragraph are shown in Figure 4. It is worth noting that this setup of Noah-MP was able to closely simulate SH in spring, autumn and winter months while overestimated SH during June to September and underestimating LH in the midday during these months.

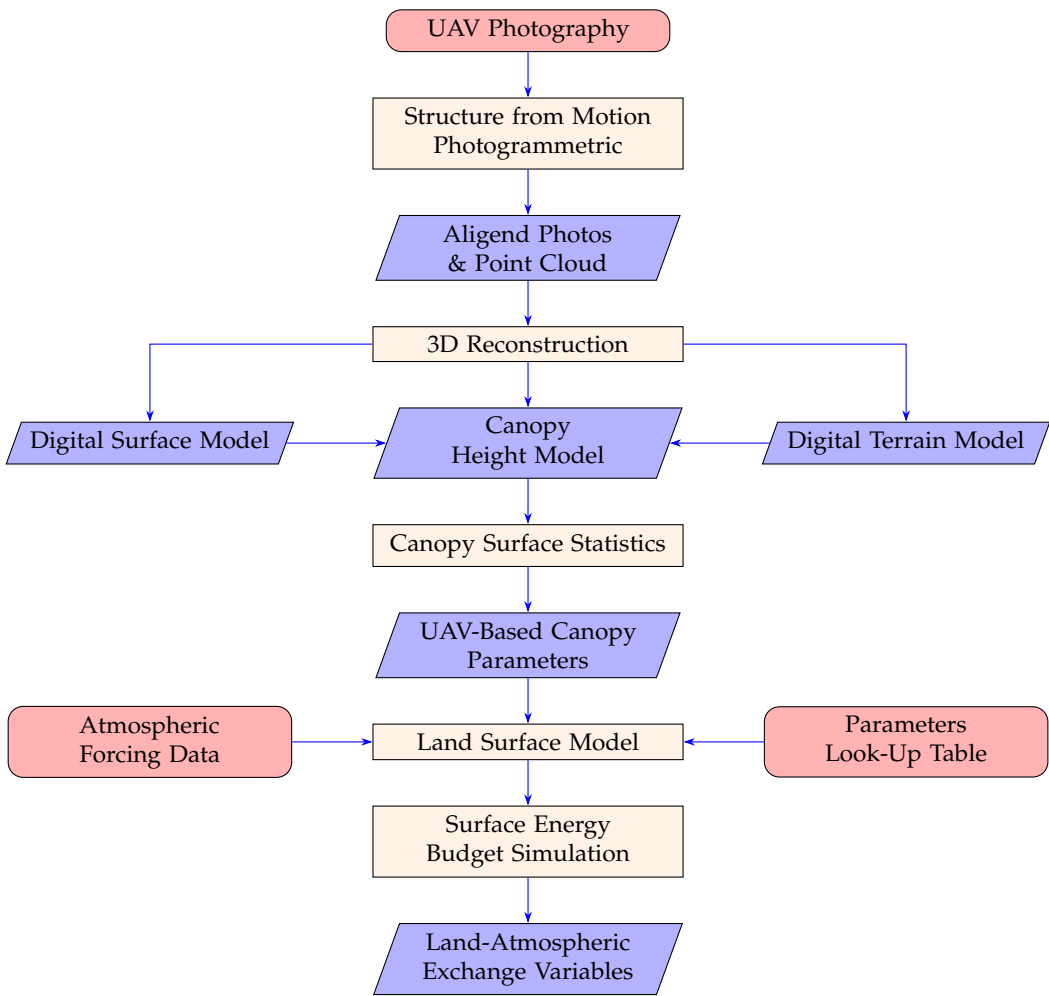


**Figure 2.** Main workflow to estimate the effects of land-air energy budget by refined canopy parameters from high-resolution UAV photography

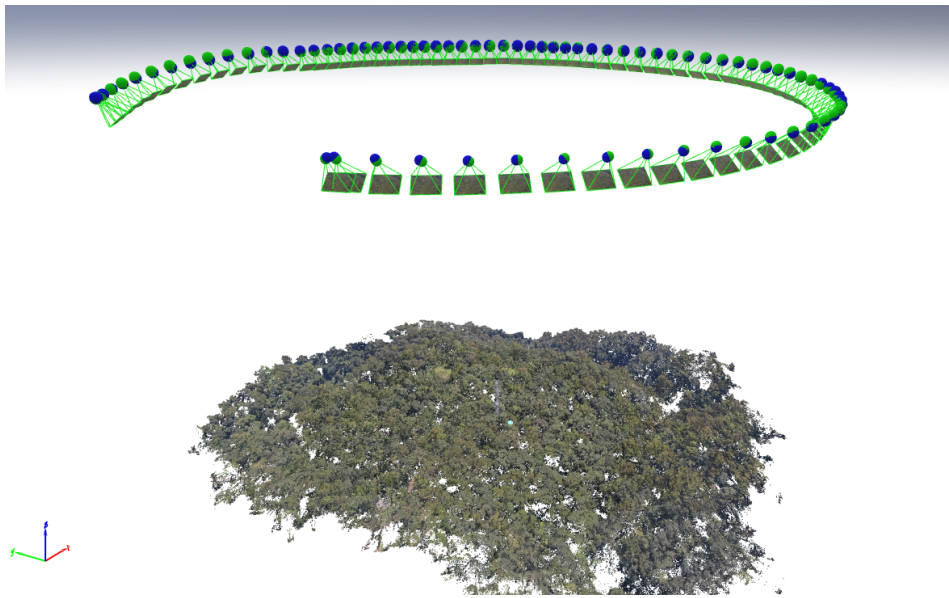


**Figure 3.** The flight lines and UAV image acquisition

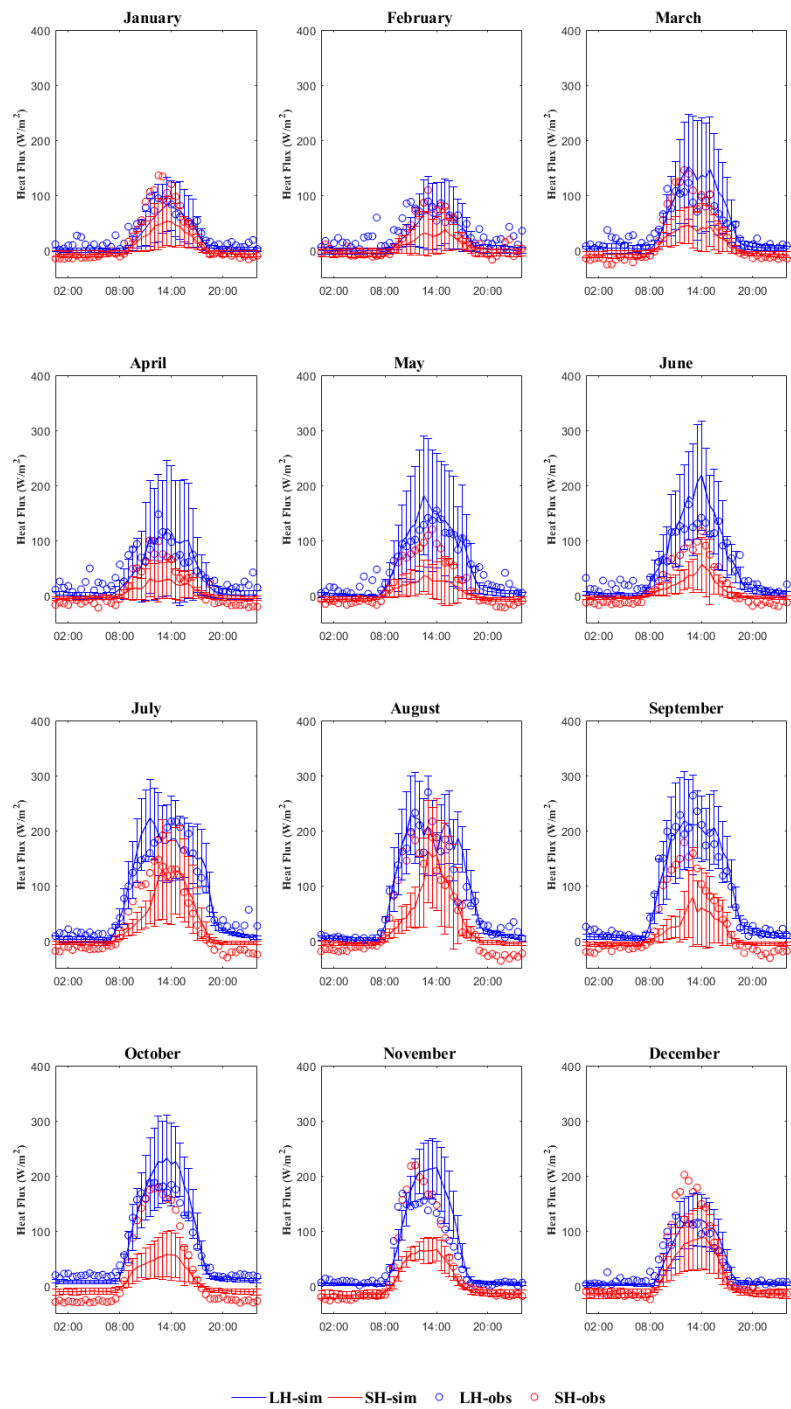


**Figure 4.** The monthly average diurnal LH and SH results from observations and simulated with the original parameters



Table 2. The set-up option of Noah-MP land surface model

Physical processes	Options	Reference
OPT_DVEG	Dynamic Vegetation Model	Dickinson <i>et al.</i> [34]
OPT_CRSS	Ball-Berry Scheme	Ball <i>et al.</i> [35]
OPT_BTR	Noah Type	Chen <i>et al.</i> [36]
OPT_RUN	SIMGM	Niu <i>et al.</i> [37]
OPT_SFC	Noah Type	Chen <i>et al.</i> [38]
OPT_RAD	$Gap = f(3D, cosz)$	Niu and Yang [39]
OPT_FRZ	NY06	Niu and Yang [40]
OPT_INF	NY06	Niu and Yang [40]
OPT_ALB	CLASS	Verseghy [41]
OPT_SNF	Jordan	Jordan [42]
OPT_TBOT	Original Noah	Barlage <i>et al.</i> [43]
OPT_STC	Semi-Implicit	Niu <i>et al.</i> [11]

3. Results and Discussion

3.1. Comparison of UAV-Based and Model-Original Canopy Parameters

The description of forest canopy characteristics in land surface model was still set by a landcover map with an attribute lookup table, although the observation techniques have significantly improved the ability to determine canopy-structure variables over large areas. As shown in Figure 5, the forests were divided into five classifications in Noah-MP model which included deciduous broadleaf forest, deciduous needleleaf forest, evergreen broinadleaf forest, evergreen needleleaf forest and mixed forest. The main difference among these forest types were the tree canopy top height, canopy bottom height and the crown radius. The quantities of tree heights and crown radius observed by UAV method were also present in Figure 5. It shows that the distribution of DHS forest appeared two stages which could indicate the characteristic as a successional subtropical forest. Compared with lidar, the ability of visible light photographs in this study to acquire the forest interlayer structure was still insufficient [21].

Additionally, the histograms of these two parameters (tree heights and crown radius) are shown in Figure 6, and the corresponding distributions were fitted as Weibull or Burr dist while the functions and coefficients were listed in Table 3. It can be seen from Figure 6 that the medians (standard deviations) of tree height and crown radius are  $12.2 \pm 5.4m$  and  $1.9 \pm 1.5m$ , respectively. These features were replaced into the attribute look-up table and then drive the Noah-MP model, which would be further discussed in section 3.2 and 3.3.

Table 3. Fitted coefficients for the distribution of UAV-based canopy parameters

Canopy Parameter	Dist Type	Functions	Coefficients
Tree Height	Weibull	$f(x a,b) = \frac{b}{a} (\frac{x}{a})^{b-1} e^{-(x/a)^b}$	$a = 14.26, b = 2.44$
Crown Radius	Burr	$f(x a,c,k) = 1 - \frac{1}{(1+(\frac{x}{a})^c)^k}$	$a = 1.46, c = 4.73, k = 0.44$

3.2. Performance on Surface Energy Budget Simulation

The effect for replacing the model-original canopy parameters with the results obtained from UAV on the surface energy components is shown in Figure 7. It can be seen that after replacing parameters, most of sensible heat, letant heat and soil heat flux were not significantly changed, and only a few points exceeded the threshold line (black dash line in Figure 7(a)), which were corresponding to the significant change. After using more accurate canopy parameters, the sensible heat flux (SH) changed at a range from  $-5.5W/m^2$  to  $1.7W/m^2$  with the slightly decreased mean ( $-0.2W/m^2$ ); the latent heat flux (LH) changed at a range from  $-0.4W/m^2$  to  $6.1W/m^2$  with the slightly increased mean ( $0.7W/m^2$ ), and the ground heat flux was basically stable in the mean value of  $2.7 \times 10^{-5}W/m^2$ . Additionally, as shown in Figure 7(b), the three components of latent heat were increasing, and the order from high to low was as the following sequence: ground evaporative heat to atmosphere ( $-3.8W/m^2 \sim 0.47W/m^2 \sim 10.0W/m^2$ ), transpiration flux ( $-1.2W/m^2 \sim 0.09W/m^2 \sim 0.16W/m^2$ ) and vegetation canopy evaporative heat to atmosphere ( $-0.3W/m^2 \sim 0.07W/m^2 \sim 1.9W/m^2$ ).

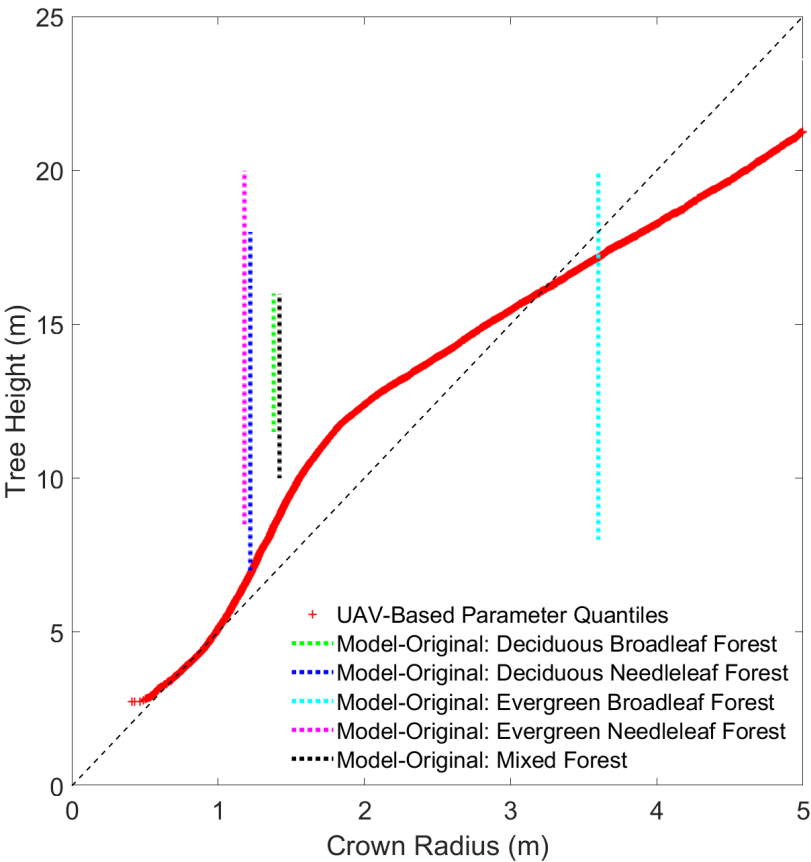


Figure 5. The distribution of UAV-based canopy parameters and model-original look-up table value

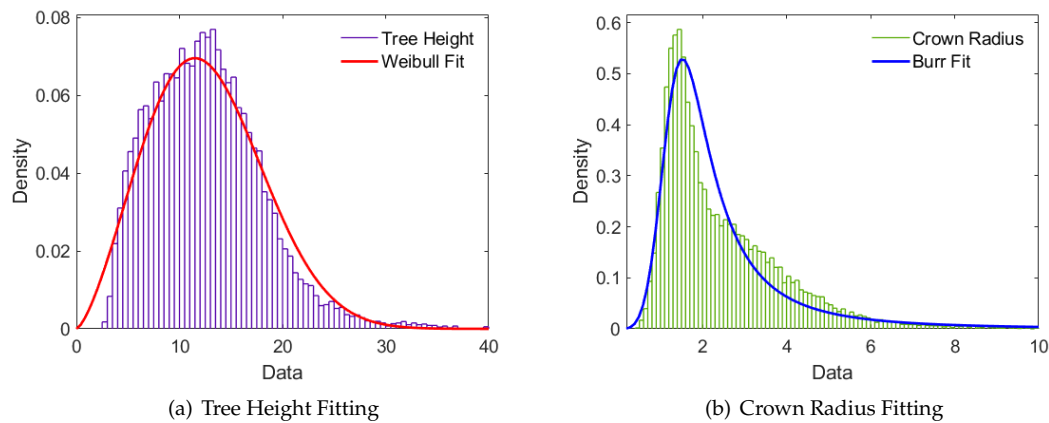
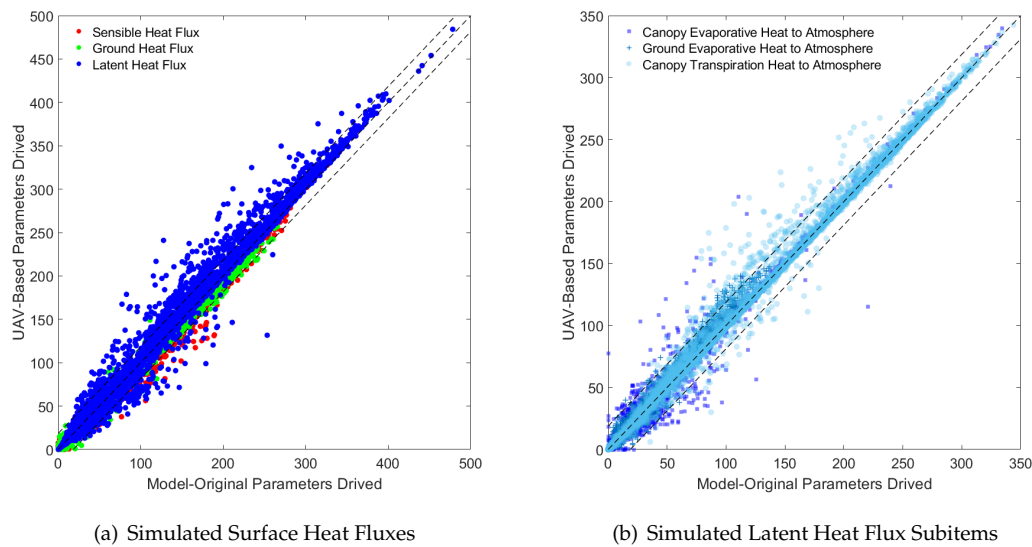


Figure 6. Histogram and distribution fits of UAV-based canopy parameters



**Figure 7.** Comparison of surface heat fluxes items from different driving

Furthermore, in order to see the more detailed impact, energy fluxes simulated by the UAV-based canopy parameters driven and model-original values driven models were compared in terms of the hourly averages through the diurnal cycle. Figure 8 shows the diurnal variation of sensible heat, ground heat and latent heat fluxes. It can be found that all these three energy components presented the significant diurnal variations, and the corresponding curves appeared with a single peak at noon and close to zero or negative value at night.

On the other hand, Figure 8 also shows the diurnal changes of surface heat fluxes from different driving. It indicated that the replacement of canopy parameters using UAV-based results could mainly have effect on latent heat during day and night while it would influence the sensible heat and ground heat in the opposite direction at night. After replacing canopy parameters with UAV-based results, the simulated latent heat flux could decrease up to -11% in the midday while increase up to 15% in the nighttime. This was probably due to the improvement of canopy characteristics which directly affected the calculation of canopy stomata [17].

Moreover, while the ground heat flux increased about 5% ~ 30% at the same time and showed an increasing trend in the daytime, the sensible heat flux decreased about 10% ~ 60% at nighttime. At the time of the day and night boundary, the sensible heat flux and the ground heat flux showed the largest change which might be due to the breakage of the boundary layer [44]. High sensitivity of canopy height for evapotranspiration was also reported in previous study [45]. Although the changes of surface heat budgets in their and our studies have similarly shown a small range, the description for the canopy characteristics of the land surface model still needs to be improved due to the expression of heterogeneity for underlying surface were overlooked.

### 3.3. Issues Related to Canopy Exchange Coefficients

To understand the influence of canopy parameters on the above-mentioned surface energy changes, we extracted the simulated results of canopy exchange coefficient. As shown in Figure 9(a), for the canopy heat exchange coefficient, the parameters driven by UAV measurement could increase about 0.5 ~ 2% compared with that of the default model. This would be the main reason for the change of surface sensible heat simulation.

At the same time, Figure 9(b) shows the simulation results of the canopy momentum exchange coefficient. It can be seen that after changing the parameters of canopy height and crown radius, the exchange coefficient of momentum could increase nearly 5% during the daytime. As the momentum



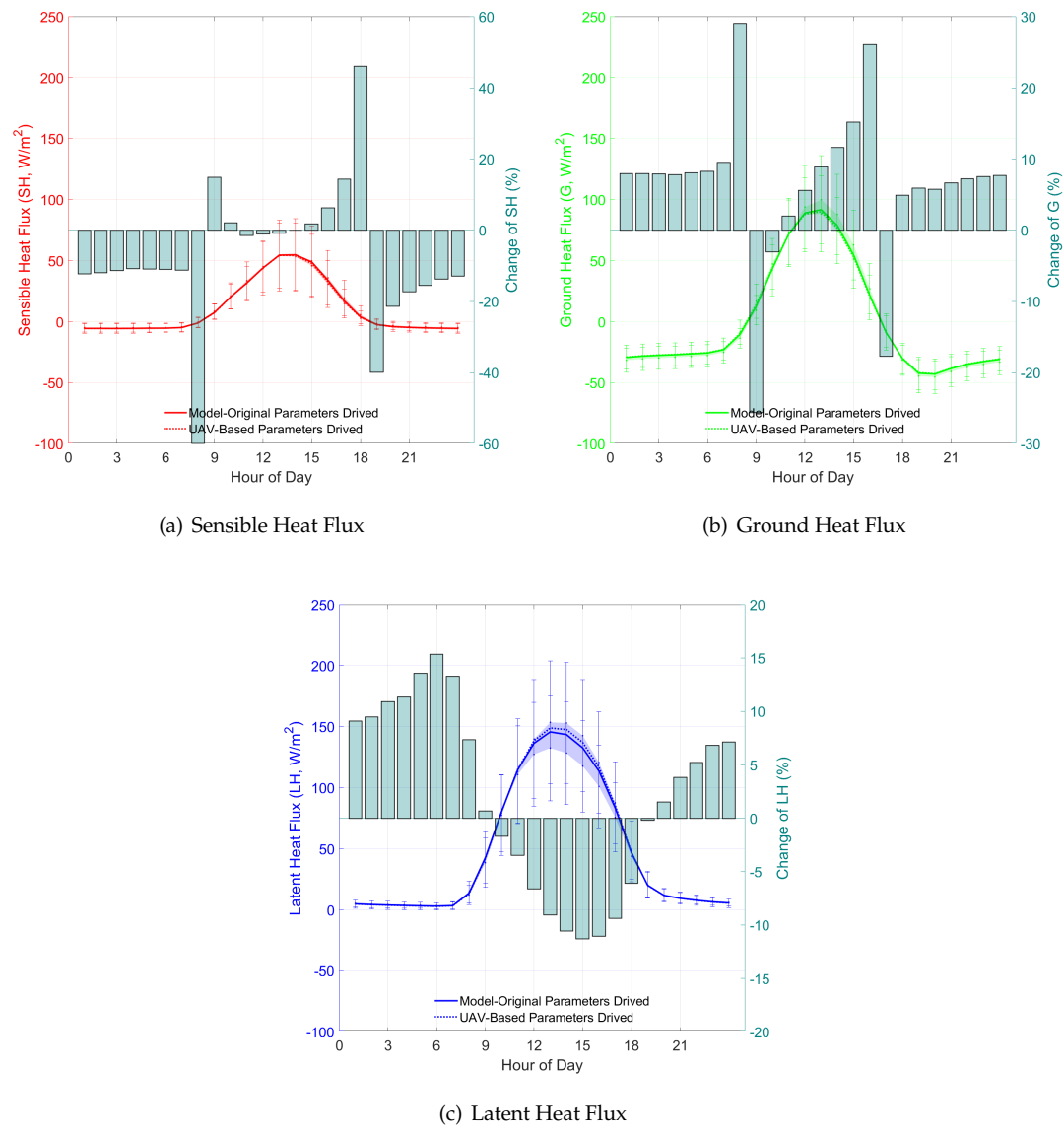


**Figure 8.** Diurnal changes of surface heat fluxes from different driving

exchange coefficient of canopy was calculated by aerodynamic resistance for momentum over canopy, it might have an impact on the variation of wind speed in the canopy. However, because the model cannot deliver the wind profiles inside and outside the canopy, the mesoscale meteorological model in the next phase should be carried out to investigate its effect on turbulence dissipation.

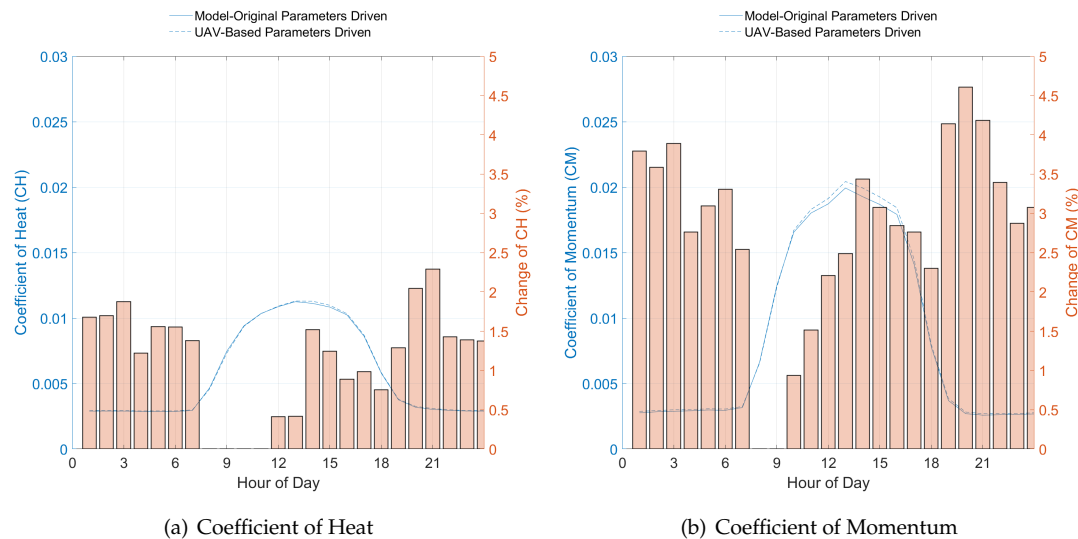


**Figure 9.** Distribution of simulated canopy exchange coefficients

### 3.4. Issues Related to Vegetation Variables

The Noah-MP land surface model includes a routine calculation for the dynamic simulation of vegetation carbon assimilation processes, while a 3-D vegetation model in the radiation transfer scheme uses canopy height to compute the total available energy at the vegetation surfaces [46]. Figure 10 shows the simulated vegetation variables of Noah-MP land surface model. It indicated that the input of UAV observed canopy height and radius could increase the average leaf area index about  $1.58 \times 10^{-2}$ , stem area index about  $1.1 \times 10^{-3}$  and green vegetation fraction about  $1.8 \times 10^{-3}$  during the simulated period. The variation mainly appeared on right sides of each frequency peak of above variables which means the more accurate canopy parameters input can restrict and improve the estimation of vegetation carbon assimilation processes inside land surface model. These results could influence the temperature and the vegetation growth characteristics [47].

## 4. Conclusions

In this study, a method to obtain local canopy parameters by unmanned aerial vehicle's photogrammetry was applied, and then a simulation with the Noah-MP model was performed over a typical subtropical forest area in South China. The results demonstrated that this method could represent the description of forest canopy characteristics more detailed. The canopy height in CN-Din area was fitted as Weibull distribution while the canopy radius followed Burr distribution; the medians (standard deviations) of UAV-based tree height and crown radius were  $12.2 \pm 5.4m$  and  $1.9 \pm 1.5m$ , respectively. Overall, it indicated that this method had strong deliverability, reasonable cost and acceptable precision, which could obtain the forest land surface parameters of several square kilometers and improve the land surface model.

The update of these local canopy parameters would significantly affect the simulation of energy fluxes, especially for the latent heat flux which could decrease up to -11% in the midday while increase up to 15% in the nighttime. Additionally, the sensible heat flux decreased about 10% ~ 60% at nighttime, while the ground heat flux increased about 5% ~ 30% at the same time, which showed an

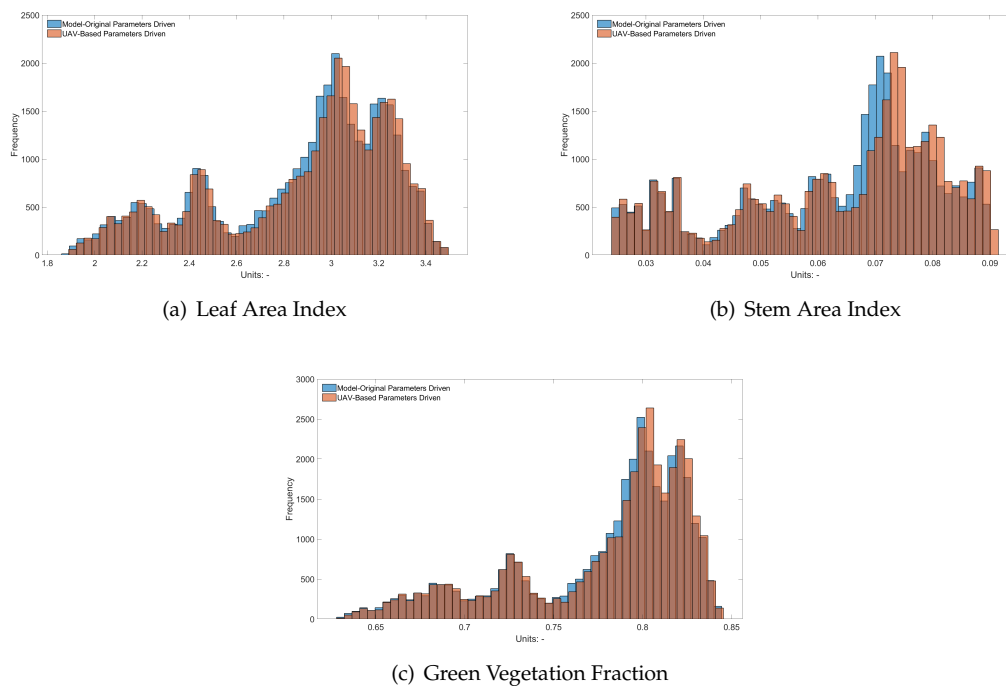


**Figure 10.** Distribution of simulated vegetation features

increase trend during the daytime. Furthermore, the update of local canopy parameters could also change canopy heat exchange coefficient through the slight increase of vegetation variables.

Although the changes of surface heat budgets have shown a small range, the description of the canopy characteristics of the land surface model still needs to be improved. Moreover, the update of canopy parameters could increase the exchange coefficient of momentum nearly 5% during the daytime. Finally, the calculation of the total available energy at the vegetation surfaces showed that the input of UAV observed canopy height and radius could increase the average leaf area index about  $1.58 \times 10^{-2}$ , stem area index about  $1.1 \times 10^{-3}$  and green vegetation fraction about  $1.8 \times 10^{-3}$  during the simulated period.

**Author Contributions:** Conceptualization, Ming Chang; Formal analysis, Jiachen Cao, Bingyin Chen and Qi Zhang; Methodology, Ming Chang; Software, Shengjie Zhu; Supervision, Xuemei Wang; Validation, Jiachen Cao, Bingyin Chen and Qi Zhang; Visualization, Shengjie Zhu; Writing – original draft, Ming Chang; Writing – review & editing, Weihua Chen, Shiguo Jia and Padmaja Krishnan.

**Funding:** This research was funded by National Key Research and Development Plan grant number 2017YFC0210103, National Natural Science Foundation grant number 41705123, Special Fund Project for Science and Technology Innovation Strategy of Guangdong Province grant number 2019B121205004, Funding from the Research Center on Low-carbon Economy for Guangzhou Region grant number 20JNZS46, Environmental Scientific Research Project in Shenzhen grant number GXZX-19042SZGK.

**Acknowledgments:** This work was supported by the Dinghushan Forest Ecosystem Research Station, Chinese Academy of Sciences and the High Performance Public Computing Service Platform of Jinan University.

**Conflicts of Interest:** The authors declare no conflict of interest.

## References

1. Pitman, A. The evolution of, and revolution in, land surface schemes designed for climate models. *International Journal of Climatology* **2003**, *23*, 479–510.
2. Chen, F.; Kusaka, H.; Bornstein, R.; Ching, J.; Grimmond, C.; Grossman-Clarke, S.; Loridan, T.; Manning, K.W.; Martilli, A.; Miao, S.; others. The integrated WRF/urban modelling system: development, evaluation, and applications to urban environmental problems. *International Journal of Climatology* **2011**, *31*, 273–288.

3. Fang, H.; Baret, F.; Plummer, S.; Schaepman-Strub, G. An overview of global leaf area index (LAI): Methods, products, validation, and applications. *Reviews of Geophysics* **2019**, *57*, 739–799.
4. Chang, M.; Fan, S.; Wang, X. Impact of refined land-cover data on WRF performance over the Pearl River Delta region, China. *Huanjing Kexue Xuebao/Acta Scientiae Circumstantiae* **2014**, *34*, doi:10.13671/j.hjkxxb.2014.0558.
5. Eagleson, P.S. *Land surface processes in atmospheric general circulation models*; Cambridge University Press, 2011.
6. Yin, G.; Li, J.; Liu, Q.; Fan, W.; Xu, B.; Zeng, Y.; Zhao, J. Regional leaf area index retrieval based on remote sensing: The role of radiative transfer model selection. *Remote Sensing* **2015**, *7*, 4604–4625.
7. Xue, Y.; Sellers, P.; Kinter, J.; Shukla, J. A simplified biosphere model for global climate studies. *Journal of Climate* **1991**, *4*, 345–364.
8. Chen, F.; Dudhia, J. Coupling an advanced land surface–hydrology model with the Penn State–NCAR MM5 modeling system. Part I: Model implementation and sensitivity. *Monthly weather review* **2001**, *129*, 569–585.
9. Xiu, A.; Pleim, J.E. Development of a land surface model. Part I: Application in a mesoscale meteorological model. *Journal of Applied Meteorology* **2001**, *40*, 192–209.
10. Mitchell, K. The community Noah land-surface model (LSM). *User's Guide Public Release Version* **2005**, *2*.
11. Niu, G.Y.; Yang, Z.L.; Mitchell, K.E.; Chen, F.; Ek, M.B.; Barlage, M.; Kumar, A.; Manning, K.; Niyogi, D.; Rosero, E.; others. The community Noah land surface model with multiparameterization options (Noah-MP): 1. Model description and evaluation with local-scale measurements. *J. Geophys. Res. D: Atmos* **2011**, *116*.
12. Ke, Y.; Leung, L.; Huang, M.; Coleman, A.M.; Li, H.; Wigmosta, M.S. Development of high resolution land surface parameters for the Community Land Model. *Geoscientific Model Development* **2012**, *5*, 1341.
13. Smirnova, T.G.; Brown, J.M.; Benjamin, S.G.; Kenyon, J.S. Modifications to the rapid update cycle land surface model (RUC LSM) available in the weather research and forecasting (WRF) model. *Monthly weather review* **2016**, *144*, 1851–1865.
14. Baldocchi, D.D.; Hicks, B.B.; Camara, P. A canopy stomatal resistance model for gaseous deposition to vegetated surfaces. *Atmospheric Environment (1967)* **1987**, *21*, 91–101.
15. Droppo, J.G. *Improved Formulations for Air-Surface Exchanges Related to National Security Needs: Dry Deposition Models*; Citeseer, 2006.
16. Huang, D.; Knyazikhin, Y.; Wang, W.; Deering, D.W.; Stenberg, P.; Shabanov, N.; Tan, B.; Myneni, R.B. Stochastic transport theory for investigating the three-dimensional canopy structure from space measurements. *Remote Sensing of Environment* **2008**, *112*, 35–50.
17. Ma, Y.; Liu, H. An advanced multiple-layer canopy model in the WRF model with large-eddy simulations to simulate canopy flows and scalar transport under different stability conditions. *Journal of Advances in Modeling Earth Systems* **2019**, *11*, 2330–2351.
18. Gan, Y.; Liang, X.Z.; Duan, Q.; Chen, F.; Li, J.; Zhang, Y. Assessment and reduction of the physical parameterization uncertainty for Noah-MP Land Surface Model. *Water Resources Research* **2019**, *55*, 5518–5538.
19. Haynes, K.; Baker, I.; Denning, S. Simple Biosphere Model version 4.2 (SiB4) technical description **2020**.
20. Weiss, M.; Baret, F. Using 3D point clouds derived from UAV RGB imagery to describe vineyard 3D macro-structure. *Remote Sensing* **2017**, *9*, 111.
21. Guo, Q.; Su, Y.; Hu, T.; Zhao, X.; Wu, F.; Li, Y.; Liu, J.; Chen, L.; Xu, G.; Lin, G.; others. An integrated UAV-borne lidar system for 3D habitat mapping in three forest ecosystems across China. *International journal of remote sensing* **2017**, *38*, 2954–2972.
22. Liu, K.; Shen, X.; Cao, L.; Wang, G.; Cao, F. Estimating forest structural attributes using UAV-LiDAR data in Ginkgo plantations. *ISPRS journal of photogrammetry and remote sensing* **2018**, *146*, 465–482.
23. McNeil, B.E.; Pisek, J.; Lepisk, H.; Flamenco, E.A. Measuring leaf angle distribution in broadleaf canopies using UAVs. *Agricultural and Forest Meteorology* **2016**, *218*, 204–208.
24. Jiménez López, J.; Mulero-Pázmány, M. Drones for conservation in protected areas: present and future. *Drones* **2019**, *3*, 10.
25. Chung, C.H.; Huang, C.y. Hindcasting tree heights in tropical forests using time-series unmanned aerial vehicle imagery. *Agricultural and Forest Meteorology* **2020**, p. 108029.

26. Brüllhardt, M.; Rotach, P.; Schleppi, P.; Bugmann, H. Vertical light transmission profiles in structured mixed deciduous forest canopies assessed by UAV-based hemispherical photography and photogrammetric vegetation height models. *Agricultural and Forest Meteorology* **2020**, *281*, 107843.
27. Chang, M.; Liao, W.; Wang, X.; Zhang, Q.; Chen, W.; Wu, Z.; Hu, Z. An optimal ensemble of the Noah-MP land surface model for simulating surface heat fluxes over a typical subtropical forest in South China. *Agricultural and Forest Meteorology* **2020**, *281*, 107815.
28. Yan, J.H.; Zhou, G.Y.; Zhang, D.Q.; Tang, X.L.; Wang, X. Different patterns of changes in the dry season diameter at breast height of dominant and evergreen tree species in a mature subtropical forest in South China. *Journal of Integrative Plant Biology* **2006**, *48*, 906–913.
29. Zhou, G.; Guan, L.; Wei, X.; Zhang, D.; Zhang, Q.; Yan, J.; Wen, D.; Liu, J.; Liu, S.; Huang, Z.; others. Litterfall production along successional and altitudinal gradients of subtropical monsoon evergreen broadleaved forests in Guangdong, China. *Plant Ecology* **2007**, *188*, 77–89.
30. Yu, X.; Pan, Y.; Song, W.; Li, S.; Li, D.; Zhu, M.; Zhou, H.; Zhang, Y.; Li, D.; Yu, J.; others. Wet and Dry Nitrogen Depositions in the Pearl River Delta, South China: Observations at Three Typical Sites With an Emphasis on Water-Soluble Organic Nitrogen. *Journal of Geophysical Research: Atmospheres* **2020**, *125*, e2019JD030983.
31. Puliti, S.; Talbot, B.; Astrup, R. Tree-stump detection, segmentation, classification, and measurement using unmanned aerial vehicle (UAV) imagery. *Forests* **2018**, *9*, 102.
32. Larrinaga, A.R.; Brotons, L. Greenness Indices from a Low-Cost UAV Imagery as Tools for Monitoring Post-Fire Forest Recovery. *Drones* **2019**, *3*, 6.
33. Zhang, Q.; Chang, M.; Zhou, S.; Chen, W.; Wang, X.; Liao, W.; Dai, J.; Wu, Z. Evaluate dry deposition velocity of the nitrogen oxides using Noah-MP physics ensemble simulations for the Dinghushan Forest, Southern China. *Asia-Pacific Journal of Atmospheric Sciences* **2017**, *53*, 519–536.
34. Dickinson, R.E.; Shaikh, M.; Bryant, R.; Graumlich, L. Interactive canopies for a climate model. *Journal of Climate* **1998**, *11*, 2823–2836.
35. Ball, J.T.; Woodrow, I.E.; Berry, J.A. A model predicting stomatal conductance and its contribution to the control of photosynthesis under different environmental conditions. In *Progress in Photosynthesis Research*; Springer, 1987; pp. 221–224.
36. Chen, F.; Mitchell, K.; Schaake, J.; Xue, Y.; Pan, H.L.; Koren, V.; Duan, Q.Y.; Ek, M.; Betts, A. Modeling of land surface evaporation by four schemes and comparison with FIFE observations. *J. Geophys. Res. D: Atmos* **1996**, *101*, 7251–7268.
37. Niu, G.Y.; Yang, Z.L.; Dickinson, R.E.; Gulden, L.E.; Su, H. Development of a simple groundwater model for use in climate models and evaluation with Gravity Recovery and Climate Experiment data. *J. Geophys. Res. D: Atmos* **2007**, *112*.
38. Chen, F.; Janjić, Z.; Mitchell, K. Impact of atmospheric surface-layer parameterizations in the new land-surface scheme of the NCEP mesoscale Eta model. *Boundary-Layer Meteorol.* **1997**, *85*, 391–421.
39. Niu, G.Y.; Yang, Z.L. Effects of vegetation canopy processes on snow surface energy and mass balances. *J. Geophys. Res. D: Atmos* **2004**, *109*.
40. Niu, G.Y.; Yang, Z.L. Effects of frozen soil on snowmelt runoff and soil water storage at a continental scale. *J. Hydrometeorol.* **2006**, *7*, 937–952.
41. Verseghy, D.L. CLASS—A Canadian land surface scheme for GCMs. I. Soil model. *International Journal of Climatology* **1991**, *11*, 111–133.
42. Jordan, R. A one-dimensional temperature model for a snow cover: Technical documentation for SNTHERM. 89. Technical report, Cold Regions Research and Engineering Lab Hanover NH, 1991.
43. Barlage, M.; Tewari, M.; Chen, F.; Miguez-Macho, G.; Yang, Z.L.; Niu, G.Y. The effect of groundwater interaction in North American regional climate simulations with WRF/Noah-MP. *Clim. Change* **2015**, *129*, 485–498.
44. Serafin, S.; Adler, B.; Cuxart, J.; De Wekker, S.F.; Gohm, A.; Grisogono, B.; Kalthoff, N.; Kirshbaum, D.J.; Rotach, M.W.; Schmidli, J.; others. Exchange processes in the atmospheric boundary layer over mountainous terrain. *Atmosphere* **2018**, *9*, 102.
45. Cuntz, M.; Mai, J.; Zink, M.; Thober, S.; Kumar, R.; Schäfer, D.; Schrön, M.; Craven, J.; Rakovec, O.; Spieler, D.; others. Computationally inexpensive identification of noninformative model parameters by sequential screening. *Water Resources Research* **2015**, *51*, 6417–6441.

46. Arsenault, K.R.; Nearing, G.S.; Wang, S.; Yatheendradas, S.; Peters-Lidard, C.D. Parameter sensitivity of the noah-mp land surface model with dynamic vegetation. *Journal of Hydrometeorology* **2018**, *19*, 815–830.
47. Liu, X.; Chen, F.; Barlage, M.; Zhou, G.; Niyogi, D. Noah-MP-Crop: Introducing dynamic crop growth in the Noah-MP land surface model. *Journal of Geophysical Research: Atmospheres* **2016**, *121*, 13–953.